Paper:

Land Cover Change Simulations in Yangon Under Several Scenarios of Flood and Earthquake Vulnerabilities with Master Plan

Tanakorn Sritarapipat[†] and Wataru Takeuchi

The University of Tokyo
6-1 Komaba 4-chome, Meguro, Tokyo 153-8505, Japan
[†]Corresponding author, E-mail: tanakorn@iis.u-tokyo.ac.jp

Yangon is the largest city and major economic area in Myanmar. However, it is considered to have a high risk of floods and earthquakes. In order to mitigate future flood and earthquake damage in Yangon, land cover change simulations considering flood and earthquake vulnerabilities are needed to support urban planning and management. This paper proposes land cover change simulations in Yangon from 2020 to 2040 under various scenarios of flood and earthquake vulnerabilities with a master plan. In our methodology, we used a dynamic statistical model to predict urban expansion in Yangon from 2020 to 2040. We employed a master plan as the future dataset to enhance the prediction of urban expansion. We applied flood and earthquake vulnerabilities based on multi-criteria analysis as the areas vulnerable to disaster. We simulated land cover changes from 2020 to 2040 considering the vulnerable areas with a master plan for multiple scenarios. The experiments indicated that by using a master plan, some of the predicted urban areas are still located in areas highly vulnerable to floods and earthquakes. By integrating the prediction of urban expansion with flood and earthquake vulnerabilities, the predicted urban areas can effectively avoid areas highly vulnerable to floods and earthquakes.

Keywords: prediction of urban expansion, disaster risk assessment, disaster risk reduction, Landsat

1. Introduction

Yangon, formerly known as Rangoon, is the largest city in Myanmar. With a population of more than five million, it is triple the size of the country's second-largest city, Mandalay [1, 2]. Yangon functions as the economic center of the country with 12% of the national population and 22% of the country's gross domestic product (GDP), based on data from the Planning Department, Ministry of National Planning and Economic Development (MNPED, 2010–2011). Yangon is considered to be the country's commercial and financial hub as well as its gateway for tourism. Yangon is expected to continue capturing a dominant share of Myanmar's economic growth. Yangon's population growth rapidly increased in the past decade. The average population growth rate of Yangon between 1998 and 2011 was 2.58% annually; the national population growth rate was 0.9% during that time [3].

However, Yangon has suffered from the series of floods, with new flooding almost every year: 2008, 2010, 2013, 2014 and 2015. In 2014, Yangon had losses of more than 8.5 million US dollars with 63,082 people, 18 schools, 17 miles of road, 8 bridges, and 56,486 acres of farmland affected [4]. In extreme cases, flooding has occurred 6 to 10 times a year when heavy rainfall has come with high tides during the monsoon season [5].

Also, Yangon was struck by earthquake in 1930, an earthquake with the magnitude of 7.0 in the Bago region and caused extensive damage, including 500 casualties. In Yangon, 50 people died out of a population of 400,000 [4]. Yangon is also a highly earthquake-prone area, located along the active Sagaing fault system and built on weak surface geological conditions associated with an alluvial delta [5].

Yangon is regarded to have high risk of floods and earthquakes. As a result, flood and earthquake aspects should be used for land use planning. In order to support urban planning and management, multiple scenarios for predicted land cover changes in Yangon from 2020 to 2040, scenarios considering flood and earthquake vulnerabilities are required to reduce the future impacts of floods and earthquakes.

Many urban expansion models have been developed in order to understand the system of urban expansion and predict which areas will be urbanized in the future. An urban land-use model based on a spatial interaction model was developed by Lowry [6]. The statistical model was used to produce an urban expansion model [7]. An urban growth model based on automata cellular was proposed by Batty [8]. Moreover, by using a multi-agent-based model, a residential distribution estimate was developed [9]. However, most works have not utilized a disaster aspect for urban expansion modeling in sustainable urban development.

This research proposes simulated urban expansion models by integrating flood and earthquake vulnerabili-

ties in order to reduce future flood and earthquake damage. By using the simulations, future urban areas will be located in areas that would be safe from floods and earthquakes. In this research, we propose the simulated land cover changes in Yangon from 2020 to 2040 under multiple scenarios of flood and earthquake vulnerabilities with a master plan.

2. Methodology

2.1. Flowchart of our Methodology

As our dataset, we used remotely-sensed data and GIS in this research. For remote sensing data, we used Landsat images with a Landsat-3 MMS image from 1978, a Landsat-4 TM image from 1990, a Landsat-7 ETM image from 2000, a Landsat-5 TM image from 2009, and a Landsat-8 OLI image from 2015 to classify land cover images. We applied SRTM DEM v. 4.1 to provide elevation, slope, flow accumulation, and the drainage network. We used TRMM 3B-43 to obtain the rainfall rate, or how much rain falls over a period of time. We employed MODIS MOD09Q1 from 2000 to 2015 to provide the historical water surface. For GIS data, we used roads in 2012 by JICA, railways in 2012 by JICA, the seismic intensity in 2012 by Thant, soil type in 2002 by the Myanmar Agriculture Service, and the 2016 master plan by JICA.

For our methodology, we developed urban expansion modeling based on a dynamic statistical model to predict land cover changes in Yangon from 2020 to 2040. We then employed the master plan as the future dataset to enhance the predictions of land cover changes from 2020 to 2040. We proposed assessments of flood and earthquake vulnerabilities based on the multiple criteria analysis for the areas vulnerable to flood and earthquake. We simulated land cover changes from 2020 to 2040 taking into consideration flood and earthquake vulnerabilities with the master plan as multiple scenarios. To validate the results, we calculated total flood and earthquake losses in area terms and then compared the multiple scenarios. **Fig. 1** is a flowchart of our methodology to simulate land cover changes from 2020 to 2040 with multiple scenarios.

2.2. Prediction of Urban Expansion

We developed urban expansion modeling based on the dynamic statistical model by using remotely sensed data and GIS data. Generally, urban expansion considers three aspects: (1) facilities such as department stores, offices, schools, etc., (2) transportation infrastructure such as roads and railways, and (3) environmental features such as rivers and mountains [10]. In this research, we defined the factors that indicate urban expansion as (1) the distance from the multiple centers of urban areas, (2) the distance from the urban areas in the past, (3) the distance from roads, (4) the distance from railways, (5) elevation, (6) the conversion of land cover, and (7) the lands separated by rivers. We used the maximum likelihood estima-
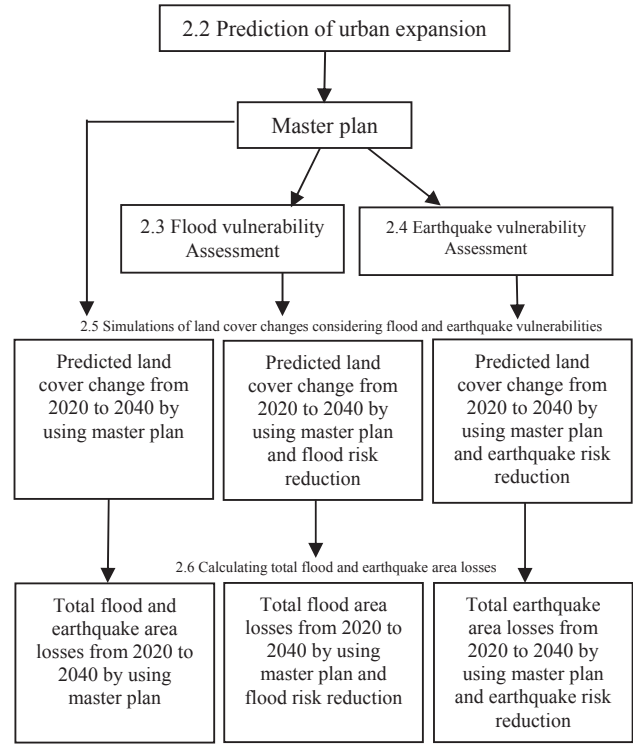
Fig. 1. Flowchart of our methodology.

tor with the dynamic statistical model to estimate urban expansion.

First, we prepared the data for urban expansion and the defined factors from remotely sensed and GIS data. For remotely sensed data, we used Landsat images from 1978, 1990, 2000, 2009, and 2015 (almost every 10 years) with the Mahalanobis distance method to classify land cover images with urban areas, farmland, forests, lakes, and rivers. The Mahalanobis distance is a well-known supervised classification method. For the training session, the sampling points were manually selected from more than five hundred samples in each class. To reduce the heavy computation in calculating the parameters of urban expansion modeling, we merged croplands and forests into vegetation, and lakes and rivers into water. Thus, there were three classes for computing in urban expansion modeling: urban areas, vegetation, and water. In this way, we could ascertain urban expansion, urban areas in the past, the conversion of land cover and lands separated by rivers. Then, we employed stereo GeoEye images from 2013 to extract building heights [11]. By combining the building heights and the separated lands, we were able to extract the multiple centers of urban areas. Next, we applied SRTM DEM as elevation. For GIS data, we used roads and railways from GIS data from 2012.

After the data was prepared, we observed the urban expansion with the defined factors to obtain the dynamic statistical values, such as the means and variances with the dynamic times.

For urban expansion modeling, we used the maximum likelihood estimator [12] with the dynamic statistical model [13]. By using the estimator, we needed to

maximize the probabilities of the defined factors using the following equation.

Maximizing Probability of the conversion of land cover +
Probability of distance from multi −
centers of urban area +
Probability of distance from urban areas in the past +
Probability of distance from road +
Probability of distance from railway +
Probability of elevation

$$\ldots \ldots \ldots \ldots \ldots \ldots \ldots \ldots \quad (1)$$

The probability of the conversion of land cover was assumed as a Markov chain. The probabilities of the distance from the multiple centers of the urban areas, the distance from the urban areas in the past, the distance from roads, the distance from railways, and land elevation were assumed as a Gaussian distribution.
Equation (1) can be separated into Eqs. (2) and (3).

Maximizing Probability of the conversion of land cover

$$\ldots \ldots \ldots \ldots \ldots \ldots \ldots \ldots \quad (2)$$

Maximizing Probability of distance from multi−
centers of urban area+
Probability of distance from urban areas in the past+
Probability of distance from road+
Probability of distance from railway+
Probability of elevation

$$\ldots \ldots \ldots \ldots \ldots \ldots \ldots \ldots \quad (3)$$

Equation (2) can be expressed in more detail as the following equation.

$$\sum_{i=1,j=1}^{m,n} vegetation(i,j,t) \rightarrow urban(i,j,t+1)$$
$$= N_{vegetation(t)\rightarrow urban(t+1)}$$

$$\sum_{i=1,j=1}^{m,n} water(i,j,t) \rightarrow urban(i,j,t+1)$$
$$= N_{water(t)\rightarrow urban(t+1)}$$

$$(4)$$

Here, $vegetation(i,j,t) \rightarrow urbanarea(i,j,t)$ is the vegetation at the pixel of i,j in time t and changes to the urban areas at the pixel of i,j in time $t+1$, $water(i,j,t) \rightarrow urbanarea(i,j,t)$ is the water at the pixel of i, j in time t and changes to the urban area at the pixel of i,j in time $t+1$, and $N_{vegetation(t)\rightarrow urban(t+1)}$ is the number of observed pixels that changed from vegetation at time t to urban at time $t+1$. $N_{water(t)\rightarrow urban(t+1)}$ is the number of observed pixels that changed from water at time t to urban at time $t+1$.

Equation (3) can be written in more detail as Eq. (5).

$$Minimizing \sum_{i=1,j=1}^{m,n} \left[\beta_1 \frac{(x_1(i,j,t+1) - \mu_1(t \rightarrow t+1,c))^2}{\sigma_1(t \rightarrow t+1,c)^2} \right.$$
$$+ \beta_2 \frac{(x_2(i,j,t+1) - \mu_2(t \rightarrow t+1))^2}{\sigma_2(t \rightarrow t+1)^2}$$
$$+ \beta_3 \frac{(x_3(i,j,t+1) - \mu_3)^2}{\sigma_3^2}$$
$$+ \beta_4 \frac{(x_4(i,j,t+1) - \mu_4(t \rightarrow t+1))^2}{\sigma_4(t \rightarrow t+1)^2}$$
$$\left. + \beta_5 \frac{(x_5(i,j,t+1) - \mu_5(t \rightarrow t+1))^2}{\sigma_5(t \rightarrow t+1)^2} \right],$$

$$\ldots \ldots \ldots \ldots \ldots \ldots \ldots \ldots \quad (5)$$

where $x_1(i,j,t) =$ the distance from the multiple centers of urban areas at the pixel of i, j in time t, $x_2(i,j,t) =$ distance from urban area in the past at the pixel of i,j in time t. $x_3(i,j,t) =$ the distance from a road at the pixel of i,j in time t. $x_4(i,j,t) =$ distance from the railway at the pixel of i,j in time t. $x_5(i,j,t) =$ elevation at the pixel of i,j in time t. $\mu_1, \mu_2, \ldots, \mu_5$ are the means of the defined factors, $\sigma_1^2, \sigma_2^2, \ldots, \sigma_5^2$ are the variances of the defined factors, and $\beta_1, \beta_2, \ldots, \beta_5$ are the precision parameters of the defined factors.

Then, in order to estimate urban expansion, Eqs. (4) and (5) were calculated simultaneously.

We used the land cover image from 1978 as the initial land cover image to estimate land cover images from 1990, 2000, and 2009.

To predict urban expansion, for a number of pixels of urban areas, we found that there was a close relationship between urban expansion and population growth as a linear function. We employed the projected population [14] with the relationship to estimate the prospective total number of pixels of urban areas. We used the observed parameters with the polynomial regression to estimate the other future parameters.

We used the estimated land cover image in 2009 as the initial land cover image to predict land cover images for 2020, 2030, and 2040.

2.3. Assessment of Flood Vulnerability

We proposed an assessment of flood vulnerability based on multi-criteria analysis in Yangon. We followed the work of Kazakis [15]. The seven factors that indicate flood vulnerability are (1) elevation, (2) slope, (3) land cover type, (4) soil type, (5) flow accumulation, (6) distance from drainage channel, and (7) rainfall rate. We used the empirical model by linking with the historical water surface from 2000 to 2015 to calculate the estimated coefficients. By using the historical water surface, the flood vulnerability indicates the vulnerable areas in terms of water surface frequency.

First, we prepared data for the defined factors and water surface from 2000 to 2015. For defined factors, we clas-

sified a Landsat image from 2015 with the Mahalanobis distance to obtain the land cover image with urban areas, croplands, forests, lakes, and rivers.

Then, we used SRTM DEM as elevation, and we employed it to calculate the slope. We also applied SRTM DEM to compute flow accumulation. Next, we used the flow accumulation to calculate drainage network. After that, we applied TRMM 3B-42 monthly data to calculate the average rainfall rate. We then used soil types from 2012 GIS data.

For the historical water surface, we used MODIS MOD09Q1 images (8 days composition) from 2000 to 2015 to provide the historical water surfaces. First, we calculated NDVI images from the MOD09Q1 images. We then classified the NDVI images into two classes of water coverage (low NDVI) and non-water coverage (high NDVI) by using the manual threshold. The historical water surface was calculated by the summation of water coverage over every 8-day period from 2001 to 2015.

We defined the flood vulnerability index on a scale of 0.0 (lowest flood vulnerability) to 1.0 (highest flood vulnerability). The flood vulnerability was defined as the linear function of the defined factors and their weights as Eq. (6) [15].

$$FVI = w_F \cdot F + w_I \cdot I + w_G \cdot G + w_U \cdot U \\ + w_S \cdot S + w_E \cdot E + w_D \cdot D, \quad (6)$$

where FVI = flood vulnerability index, F = flow accumulation, I = rainfall rate, G = soil type, U = land cover type, S = slope, E = elevation, D = distance from drainage network, and w_i = the weight of the defined factor.

We assigned the values of the parameters of the flood vulnerability index in **Table 1**.

We calculated the weights of the flood vulnerability index by using a linear regression with the historical water surface. After the calculations, the estimated weights were expressed as $w_F = -10.2$, $w_I = 29.0$, $w_G = 5.01$, $w_U = -0.06$, $w_S = 4.37$, $w_E = 59.9$, and $w_D = 3.9$.

2.4. Assessment of Earthquake Vulnerability

Following the work of Karimzadeh [16], we proposed an assessment of earthquake vulnerability based on the multi-criteria analysis in Yangon. We used soil type and slope as a linear function to calculate the seismic amplitude map (microzonation map). Then, we computed the ground shaking map by multiplying Thant's simulated seismic intensity [17] by the amplitude map. The ground shaking map was assumed as the earthquake vulnerability index.

First, we prepared data for the soil type, slope, and simulated seismic intensity. We used SRTM DEM to calculate the slope. For soil type, we used the soil type map from 2002 GIS data. For seismic intensity, we used the simulated seismic intensity with the earthquake probability of 2% from the work of Thant [17].

Then, we calculated the earthquake amplitude map. The earthquake amplitude was defined in terms of the in-

Table 1. The defined parameters of flood vulnerability index.

Parameters	Class	Index value
Flow acc. (F)	600,000-2,000,000	1.0
	60,000-600,000	0.8
	10,000-60,000	0.6
	400-10,000	0.4
	0-400	0.2
Distance. from drainage (D)	0-270	1.0
	271-540	0.8
	541-810	0.6
	811-1350	0.4
	1350-3510	0.2
Elevation [m] (E)	0-3	1.0
	4-7	0.8
	8-10	0.6
	11-17	0.4
	18-68	0.2
Land cover (U)	Urban	1.0
	Cropland	0.67
	Forest	0.33
Rainfall rate [mm/hr] (I)	0.29	0.5
Slope [%] (S)	0-0.20	1.0
	0.21-0.62	0.8
	0.63-1.19	0.6
	1.20-2.62	0.4
	2.63-14.18	0.2
Soil types (G)	Rocks	0.8
	Alluvial	0.2

Table 2. The defined parameters of earthquake amplitude index.

Parameters	Class	Index value
Soil types (G)	Alluvial	1.0
	Lateritic soil (Rock)	0.5
Slope [degree] (S)	Mean of 2.68	1.0
	Mean of 1.38	0.75
	Mean of 0.57	0.50
	Mean of 0.55	0.25

dex on a scale of 0.0 (lowest amplitude) to 1.0 (highest amplitude). The earthquake amplitude was defined as the linear function of the defined factors of (1) soil type and (2) slope. The earthquake amplitude can be expressed using the following equation.

$$EA = w_G \cdot G + w_S \cdot S + C, \quad \ldots \ldots \ldots \quad (7)$$

where EA = earthquake amplitude, G = soil type, S = slope, C = constant, w_i = the weight of the defined factor.

We assigned the values of the parameters of the earthquake amplitude index in **Table 2**.

For the weights of the earthquake amplitude index, we followed the expert opinion from the work of Karimzadeh [16]. The weight of the soil type (w_G) was 0.3, and the weight of the slope (w_S) was 0.1. In the work of Karimzadeh [16], the factors of soil type, slope, alluvial thickness, water table, and predominant period were used. However, in this research, we did not have an alluvial thickness, water table, or predominant period. As a

result, the bias (C) is 0.6 since it is expressed in terms of unobserved parameters of alluvial thickness (the weight of 0.25), water table (the weight of 0.25), and predominant period (the weight of 0.1).

Next, we used the seismic intensity map from the work of Thant [17]. The seismic hazard analysis is simulated by applying the probabilistic way. In this research, we used the seismic intensity map in terms of peak ground acceleration (PGA) with the earthquake probability of 2%.

Then, the earthquake amplitude map and the seismic intensity map were integrated to compute the ground shaking map. The equation of the ground shaking term of PGA is expressed as in the following equation.

$$GS = EA \times EI, \qquad \ldots \ldots \ldots \ldots \ldots \quad (8)$$

where GS = ground shaking, EA = earthquake amplitude, and EI = earthquake intensity.

Next, the ground shaking map was converted to the earthquake vulnerability index on a scale of 0.0 (lowest earthquake vulnerability) to 1.0 (highest earthquake vulnerability) by using a linear transformation.

2.5. Simulations of Land Cover Changes Considering Flood and Earthquake Vulnerabilities

As in Kron's work [18], disaster risk reduction can be expressed in terms of reducing (1) the hazard, (2) vulnerability, and (3) value. The hazard refers to the threatening natural disaster event, including its frequency of occurrence and its level of damage. Then, the vulnerability can refer to the vulnerable areas that are highly lacking in resistance to damaging and destructive forces. Next, the value or value at risk can refer to the buildings, items, humans, and properties that are present at the location involved.

In this research, the hazard was not considered in disaster risk reduction. Thus, disaster risk reduction are expressed in the term of reducing (1) vulnerability and (2) value as Eq. (9).

$$\textit{Disaster risk reduction} \\ = \textit{reducing Vulnerability} * \textit{Vulue}. \qquad (9)$$

We assumed that urban (high value) flight from the high disaster vulnerability area (high vulnerability) was equal to disaster risk reduction in terms of reducing vulnerability and value. Urban areas are more important areas than surrounding areas, such as vegetation and water areas, since urban areas have the characteristics of the highest population density, various human-built features, and the most important human activities. When an urban area is impacted by a disaster, it might make for a huge loss and might spread the impacts throughout the city or to the countryside. As a result, we tried to allocate urban areas in the future to the low venerability areas or safe areas to reduce the impact of loss-causing disasters.

The disaster risk reduction for future urban expansion can be expressed in terms of urban areas growing due to escaping from areas highly vulnerable to disaster. Thus, by integrating it with disaster vulnerability, the predic-
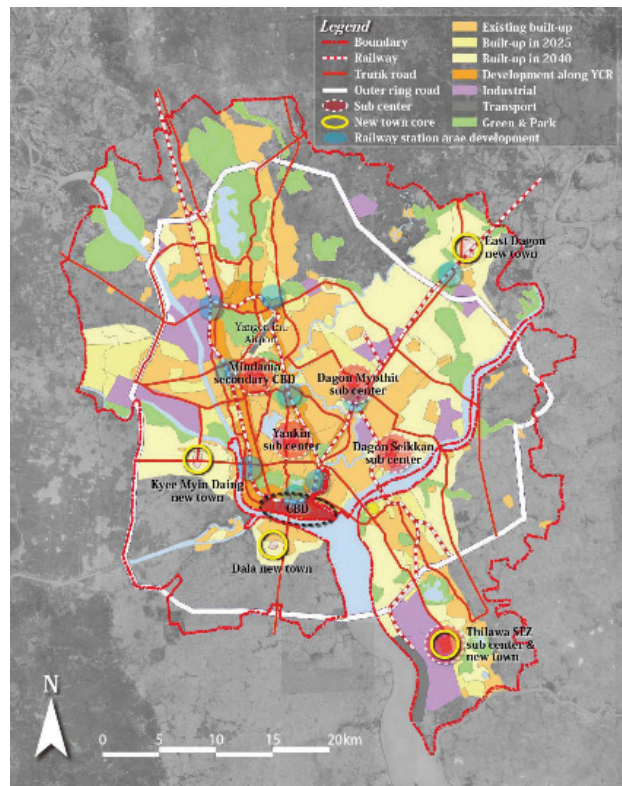
Source: JICA, 2016.

Fig. 2. The master plan in Yangon by JICA, 2016.

tion of urban expansion can be calculated by modifying an equation 5 in order to indicate the simulated urban areas that would avoid the highly vulnerable areas.

First, to make the prediction of urban expansion more reliable, the master plan can be used as the future dataset for the prediction model. The master plan for Yangon was analyzed from many aspects of urban growth by many experts and was provided by the JICA Team [19]. In the master plan, there are many features, including the new town core, subcenter, industry, transportation, built-up areas in 2025, and built-up areas in 2040 (**Fig. 2**).

Those features can be used to extract new centers of urban areas, new roads, and new railways as the future dataset for the prediction model. To make the prediction of the urban expansion as accurate as possible, we used the land cover image from 2015 as the initial image for the urban expansion estimation to predict the urban expansion in 2020, 2030, and 2040. We also used the five classes of urban area, cropland, forest, lake, and river instead of the three classes of urban area, vegetation, and water in the simulation step. We did this since the simulation process of urban expansion modeling did not have a high computation cost and forest is a significant area for preservation in the master plan.

In predicting urban expansion while considering flood vulnerability, we used the prediction of urban expansion with the master plan to get more reliable results for urban expansion in the future. In this research, the assessment of flood vulnerability was used as one factor in the prediction

model, as can be seen in Eq. (10).

$$
\begin{aligned}
Minimizing \sum_{i=1,j=1}^{m,n} \Bigg[&\beta_1 \frac{\left(x_1(i,j,t+1) - \mu_1(t \to t+1,c)\right)^2}{\sigma_1(t \to t+1,c)^2} \\
&+ \beta_2 \frac{\left(x_2(i,j,t+1) - \mu_2(t \to t+1)\right)^2}{\sigma_2(t \to t+1)^2} \\
&+ \beta_3 \frac{\left(x_3(i,j,t+1) - \mu_3\right)^2}{\sigma_3^2} \\
&+ \beta_4 \frac{\left(x_4(i,j,t+1) - \mu_4(t \to t+1)\right)^2}{\sigma_4(t \to t+1)^2} \\
&+ \beta_5 \frac{\left(x_5(i,j,t+1) - \mu_5(t \to t+1)\right)^2}{\sigma_5(t \to t+1)^2} \\
&+ \beta_6 \frac{\left(x_6(i,j)\right)^2}{\sigma_6^2} \Bigg].
\end{aligned}
$$

$$\ldots \ldots \ldots \ldots \ldots \ldots \ldots \ldots \ldots \quad (10)$$

$x_6(i,j)$ = the flood vulnerability index at the pixel of (i,j), σ_6^2 are the variances of the flood vulnerability index, and β_6 is the weight parameter of the flood vulnerability index.

By using the flood vulnerability map with the prediction of urban expansion, the predicted urban areas will try to avoid the areas highly vulnerable to floods.

In the prediction of urban expansion taking earthquake vulnerability into consideration, we also used the prediction of urban expansion with the master plan to raise the reliability of future urban expansion. In this research, the assessment of earthquake vulnerability was used as one factor in the prediction model, Eq. (11).

$$
\begin{aligned}
Minimizing \sum_{i=1,j=1}^{m,n} \Bigg[&\beta_1 \frac{\left(x_1(i,j,t+1) - \mu_1(t \to t+1,c)\right)^2}{\sigma_1(t \to t+1,c)^2} \\
&+ \beta_2 \frac{\left(x_2(i,j,t+1) - \mu_2(t \to t+1)\right)^2}{\sigma_2(t \to t+1)^2} \\
&+ \beta_3 \frac{\left(x_3(i,j,t+1) - \mu_3\right)^2}{\sigma_3^2} \\
&+ \beta_4 \frac{\left(x_4(i,j,t+1) - \mu_4(t \to t+1)\right)^2}{\sigma_4(t \to t+1)^2} \\
&+ \beta_5 \frac{\left(x_5(i,j,t+1) - \mu_5(t \to t+1)\right)^2}{\sigma_5(t \to t+1)^2} \\
&+ \beta_7 \frac{\left(x_7(i,j)\right)^2}{\sigma_7^2} \Bigg].
\end{aligned}
$$

$$\ldots \ldots \ldots \ldots \ldots \ldots \ldots \ldots \ldots \quad (11)$$

$x_7(i,j)$ = the earthquake vulnerability index at the pixel of i,j, σ_7^2 are the variances of the earthquake vulnerability index, and β_7 are the weight parameter of the earthquake vulnerability index.

By using the earthquake vulnerability map with the prediction of urban expansion, the predicted urban areas will try to avoid the areas highly vulnerable to earthquake.

2.6. Calculating Total Flood and Earthquake Losses

To evaluate the results of the predicted urban areas when a master plan is used and when a master plan plus flood risk reduction is used, we considered the total flood loss in terms of area. As put forth in Kron's work [18], disaster risk assessment can be expressed by hazard, vulnerability, and value. In this research, based on Kron's work [18], we used the following equation to define the total flood loss.

$$Total\_FLA(t) = \sum \left(LC(i,j,t) \times FVI(i,j)\right). \quad . \ (12)$$

$Total\_FLA(t)$ = total flood loss in terms of area at time t, $LC(i,j,t)$ = land cover at pixel (i,j) at time t (urban area, cropland, forest), and $FVI(i,j)$ = flood vulnerability index at pixel (i,j).

To evaluate the results of the predicted urban areas when a master plan is used and when a master plan plus flood risk reduction is used, we considered the total earthquake loss in terms of area. Based on Kron's work [18], we used the following equation to define the total earthquake loss in terms of area.

$$Total\_ELA(t) = \sum \left(LC(i,j,t) \times EVI(i,j)\right). \quad . \ (13)$$

$Total\_ELA(t)$ = total earthquake loss in terms of area at time t, $LC(i,j,t)$ = land cover at pixel (i,j) at time t (urban area, cropland, forest), and $EVI(i,j)$ = earthquake vulnerability index at pixel (i,j).

3. Results and Discussion

3.1. Prediction of Urban Expansion

The referenced land cover images from 1990, 2000, and 2009 can be seen as **Figs. 3(a)**, **(c)**, and **(e)**, respectively, and the estimated land cover images from 1990, 2000, and 2009 are presented as **Figs. 3(b)**, **(d)**, and **(f)**, respectively.

The referenced land cover image from 2015 is shown in **Fig. 4(a)**, and the predicted land cover images from 2020, 2030, and 2040 are presented as **Figs. 4(b)**, **(d)**, and **(f)**, respectively.

For validation, we made two classes: urban and non-urban. The accuracies of the estimated and predicted urban expansion images are expressed in **Table 3**.

We found the average accuracy to be 92.88% with a true positive rate of 73.31% (urban estimate) and a true negative rate of 95.07% (non-urban estimate). In the prediction of urban expansion, the urban areas look low distribution since we did not have the dataset for the future, such as for new roads and railways.

3.2. Assessment of Flood Vulnerability

The results of the flood vulnerability assessment can be seen in **Fig. 5**.

After seeing the results of the flood vulnerability assessment, we used empirical model linking with the historical water surface to investigate whether elevation had

Table 3. The accuracy of urban expansion modeling.

Year	Accuracy [%]	True Positive Rate [%]	True Negative Rate [%]
1990	98.01	77.39	99.03
2000	93.63	64.10	96.55
2009	91.39	68.76	95.06
2015	88.43	82.97	89.64
Average	92.88	73.31	95.07
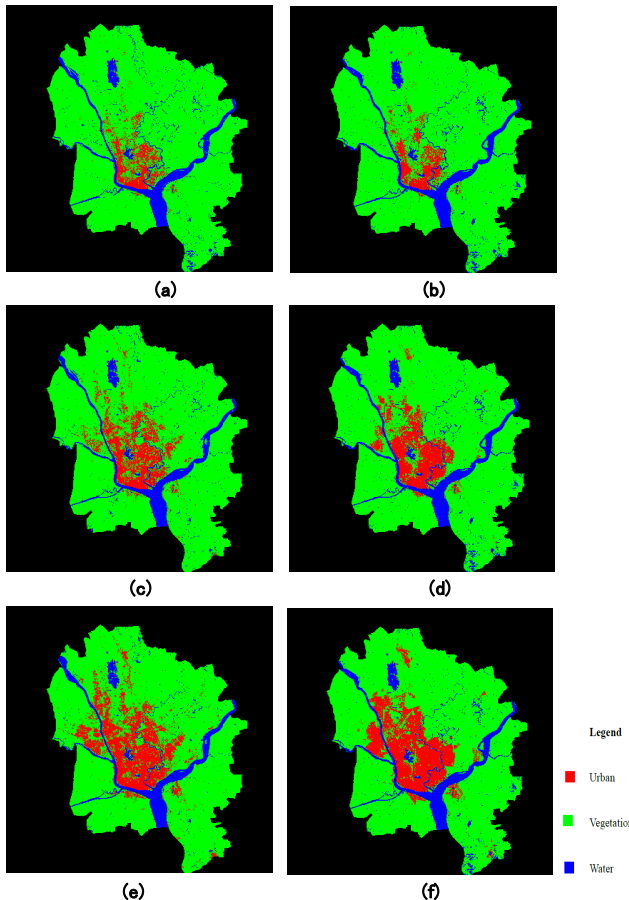
Fig. 3. The reference land cover image in (a) 1990, (c) 2000, (e) 2009 and the estimated land cover image in (b) 1990, (d) 2000, (f) 2009.

Fig. 5. Flood vulnerability map.
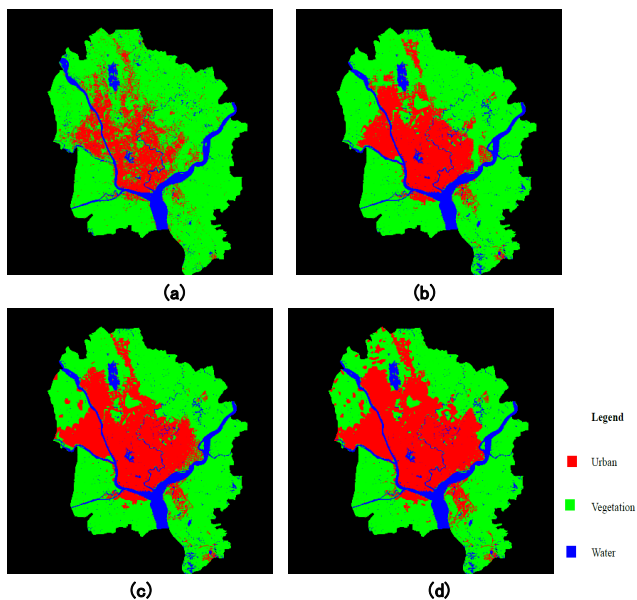
Fig. 4. The reference land cover image in (a) 2015 and the predicted land cover image in (b) 2020, (c) 2030, and (d) 2040.
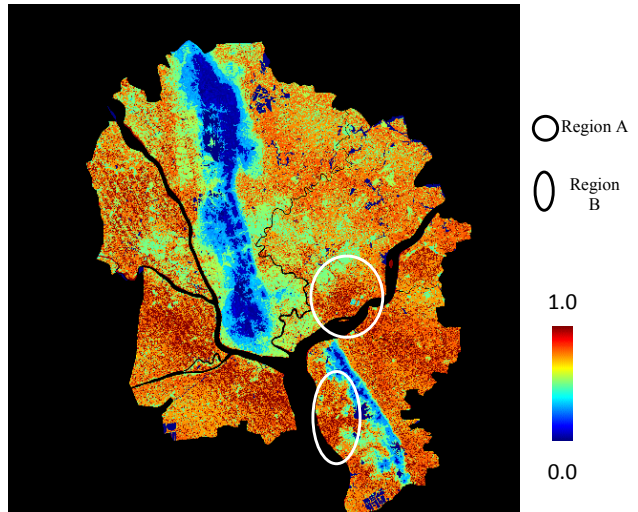
the most influence on the flood vulnerability index. However, the impacts of flow accumulation and drainage net-

works could not be detected since the estimation relies on the historical water surface as analyzed by MODIS 8 days composition which can detect water surface areas that remain more than 4 days. Consequently, our resulting flood vulnerability map concerns coastal and riverine floods and indicates vulnerable areas in terms of the frequency of the water surface.

3.3. Assessment of Earthquake Vulnerability

The results of earthquake vulnerability assessment are shown in **Fig. 6**.

According to the results of the earthquake vulnerability assessment, the areas vulnerable to earthquake can be classified into three significant areas: (1) high shaking ground areas, (2) alluvial areas, and (3) high slope areas. In Yangon, the eastward areas are highly vulnerable since they are located close to a faultline. Most areas are located in alluvial areas that have also highly vulnerable areas. However, few areas are highly vulnerable areas due to their steep slope.

3.4. Simulation of Land Cover Changes Considering Flood Vulnerability

The urban expansion images for 2020, 2030, and 2040, predicted by using the master plan, are shown in **Figs. 7(a)**, **(c)**, and **(e)**, respectively. The urban expansion
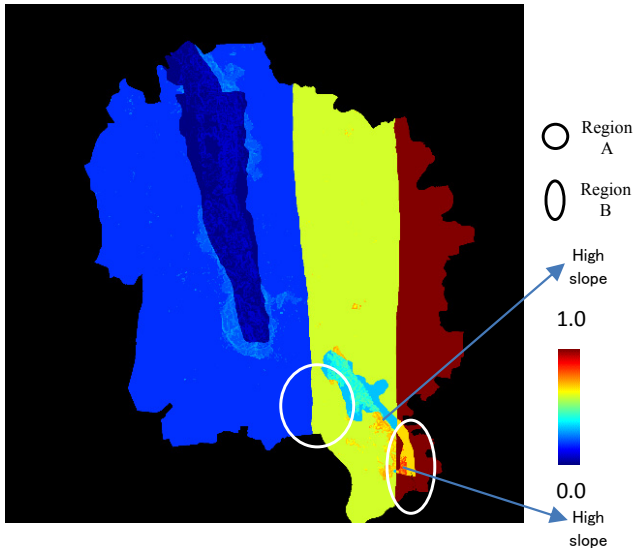
Fig. 6. Earthquake vulnerability map.
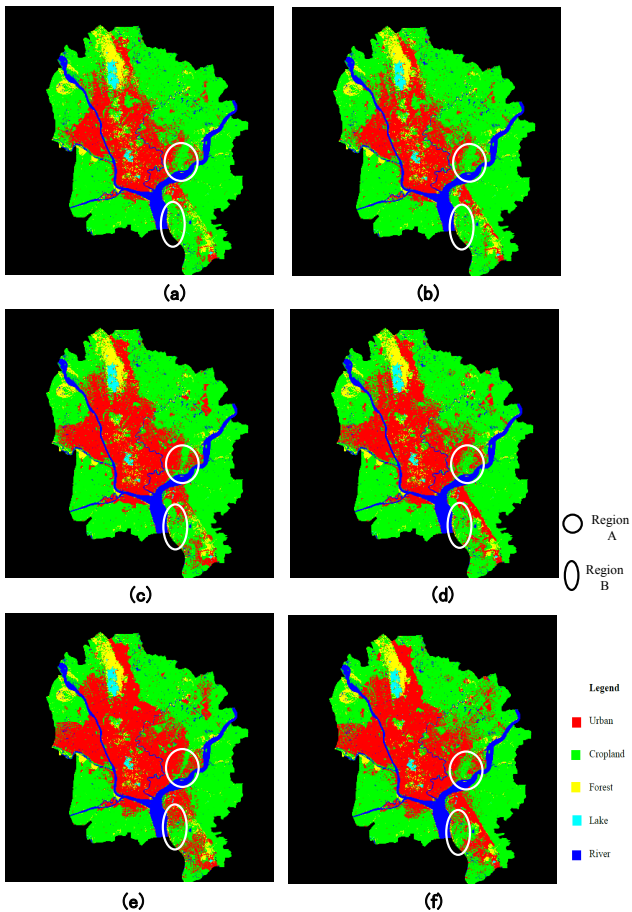
Fig. 7. The predicted land cover image in (a) 2020, (c) 2030, (e) 2040 using master plan and the predicted land cover image in (b) 2020, (d) 2030, (f) 2040 using flood risk reduction.

images in 2020, 2030, and 2040 predicted by using the master plan with the flood vulnerability map are shown in **Figs. 7(b)**, **(d)**, and **(f)**, respectively.

The total flood losses in Yangon from 2020 to 2040 in terms of area in urban areas, croplands, and forests when

Table 4. Total flood area losses from 2020 to 2040 [km^2].

Using master plan			
	2020	**2030**	**2040**
Urban	231.18	297.15	364.77
Cropland	784.23	723.23	659.23
Forest	50.21	45.25	41.62
Using master plan and flood risk reduction			
	2020	**2030**	**2040**
Urban	222.39	280.53	346.56
Cropland	793.71	742.10	680.21
Forest	49.53	42.99	38.85
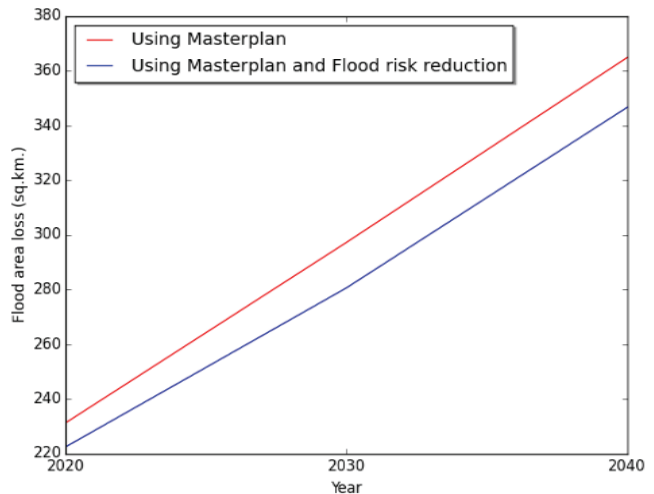
Fig. 8. Comparison of total flood area losses using master plan with and without flood risk reduction.

a master plan is used and when a master plan and flood risk reduction is used in are described in **Table 4**.

Figure 8 compares total urban flood losses in terms area using a master plan and using a master plan with flood risk reduction in Yangon from 2020 to 2040.

Table 4 and **Fig. 7** show that the total flood losses in terms of area are highest for cropland. From 2020 to 2040, the total flood losses in terms of area will have increased since the urban areas will have grown, but the total flood losses for cropland in terms of area will have decreased because the cropland areas will have shrunk, whereas the total flood losses for forests in terms of area look stable.

We found that by using a master plan with the prediction, some of the predicted urban areas are still located in highly vulnerable areas (**Figs. 7(a)**, **(c)**, and **(e)**). For example, in the southern and eastern parts of Yangon (Regions A and B in **Fig. 5**), some prospective urban areas are located in the areas highly vulnerable to flooding, mainly because they are in low elevations. By using a master plan and flood vulnerability map with the prediction, the predicted urban areas can avoid the highly vulnerable areas effectively. In **Figs. 7(b)**, **(d)**, and **(f)**, the prospective urban areas are located in the areas that are safe (high in elevation) or have low vulnerability to flooding. The statis-
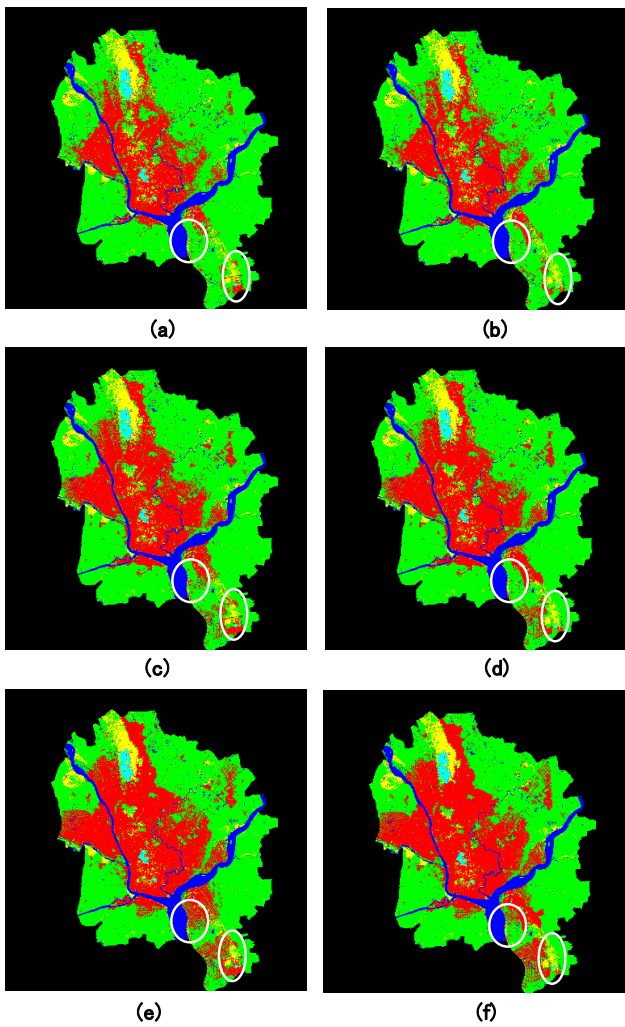
Fig. 9. The predicted land cover image in (a) 2020, (c) 2030, (e) 2040 using master plan and the predicted land cover image in (b) 2020, (d) 2030, (f) 2040 using earthquake risk reduction.

Fig. 10. Comparing the total earthquake area losses between using master plan and flood risk reduction.

tics of the total urban flood loss in terms of area (**Fig. 8**) confirmed that the values of total urban flood losses in terms of area from 2020 to 2040 obtained through integration with flood risk reduction are less than when flood risk reduction is not used by around 3.80% for 2020, 5.60% for 2030, and 5.00% for 2040.

3.5. Simulated Land Cover Change Considering Earthquake Vulnerability

The predicted land cover images obtained by using a master plan are shown in **Figs. 9(a)**, **(c)**, and **(e)**. The predicted land cover images obtained by using a master plan with the earthquake vulnerability map are shown in **Figs. 9(b)**, **(d)**, and **(f)**.

In **Table 5**, the total lost in Yangon to earthquake from 2020 to 2040 in terms of urban area, cropland, and forest when a master plan is used is compared with the data obtained using a master plan and earthquake risk reduction.

In **Fig. 10**, the total lost in Yangon to earthquake from 2020 to 2040 in terms of urban area when a master plan

is used is compared with the data obtained using master plan and earthquake risk reduction.

In **Table 5** and **Fig. 9**, we found that the total earthquake loss in terms of area is the highest for cropland. By considering with time variation from 2020 to 2040, the total area lost to earthquake for urban areas has increased, but the total area lost to earthquake for cropland areas has decreased. The total forest area lost to earthquake looks stable.

We investigated by using the masterplan with the prediction whether some of the predicted urban areas were still located in highly vulnerable areas (**Figs. 9(a)**, **(c)**, and **(e)**). For instance, in the southern parts of Yangon, some prospective urban areas are located in areas (alluvial soils) highly vulnerable to earthquake as Region A in **Fig. 6** and in the highly earthquake vulnerable areas near the faultline as Region B in **Fig. 6**. By using a master plan and earthquake vulnerability map with the prediction, the predicted urban areas can avoid highly vulnerable areas effectively (**Figs. 9(b)**, **(d)**, and **(f)**). In the southern parts of Yangon, the prospective urban areas continue to be located in areas with low vulnerability of earthquake (rock areas) as Region A and with low vulnerability of earthquake areas (far from faultlines) as Region B. The graphs of the total earthquake losses in terms of area (**Fig. 10**) confirm that the values of total earthquake losses in terms of area from 2020 to 2040 by using earthquake risk reduction are less than those without using earthquake risk reduction, around 5.02% for 2020, 4.28% for 2030, and 4.84% for 2040.

3.6. Comparison of Simulated Land Cover Changes Considering Flood and Earthquake Vulnerabilities

Figure 11 compares the predicted land cover change considering flood vulnerability (**Figs. 11(a)**, **(c)**, and **(e)**) and the predicted land cover change considering earthquake vulnerability (**Figs. 11(b)**, **(d)**, and **(f)**).
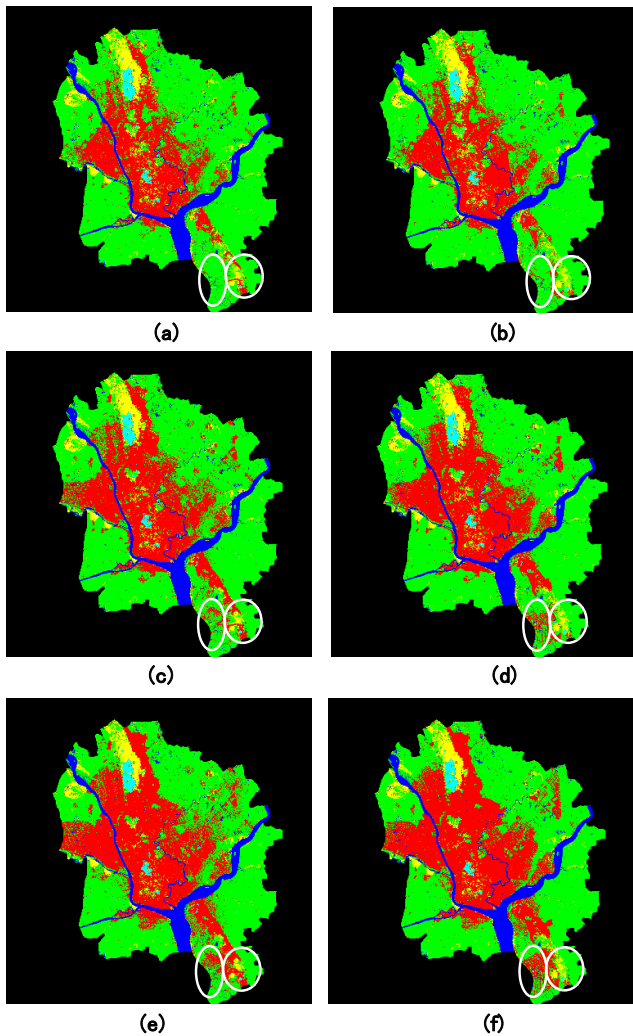
Fig. 11. The predicted land cover image in (a) 2020, (c) 2030, (e) 2040 using flood risk reduction and the predicted land cover image in (b) 2020, (d) 2030, (f) 2040 using earthquake risk reduction.

We investigated that the urban expansions by using flood vulnerability and by using earthquake vulnerability have some different results. Some areas are high vulnerable to flood but low vulnerable to earthquake. While, some areas are low vulnerable to flood but high vulnerable to earthquake. As a result, by using individually flood and earthquake risk reductions, some of the predicted urban areas will be located in lowly flood vulnerable areas but highly earthquake vulnerable areas for using flood risk reduction, whereas some of the predicted urban areas will be located in lowly earthquake vulnerable areas but highly flood vulnerable areas for using earthquake risk reduction. For example, Region A in **Fig. 11** has lowly flood vulnerable areas (high elevation) but highly earthquake vulnerable areas (near faultline). Hence, by simulating urban expansion with flood vulnerability, urban areas will be occurred in Region A (safe for flood) but by simulating urban expansion with earthquake vulnerability, urban areas will be disappeared in Region A (dangerous for earthquake). In contrast, Region B in **Fig. 11** has highly flood

vulnerable areas (low elevation) but lowly earthquake vulnerable areas (far faultline). Thus, by simulating urban expansion with flood vulnerability, urban areas will be lost in Region B (dangerous for flood) but by simulating urban expansion with earthquake vulnerability, urban areas will be appeared in Region B (safe for earthquake).

To improve the resultant urban expansion that can against both flood and earthquake, the simulated land cover change by using integrally flood and earthquake risk reduction should be conducted. However, for calculating the reliable parameters of urban expansion model by combining flood and earthquake risk reductions, there must have been more needed information such as affected population, damaged properties or economic losses by flood and by earthquake.

4. Conclusion

First, we developed an urban expansion model to predict urban expansion from 2020 to 2040 in Yangon, Myanmar. Then, we proposed flood and earthquake vulnerabilities based on a multi-criteria analysis in Yangon. Next, we demonstrated the simulations of land cover changes in Yangon from 2020 to 2040 with the multiple scenarios of flood and earthquake vulnerabilities with the master plan.

In the experiments, we found that by using the master plan with the prediction of urban expansion, the predicted urban expansion was more reliable since the master plan provides future data. Unfortunately, by using the master plan, we found some of the predicted urban areas to be located in highly vulnerable areas. However, by integrating flood and earthquake risk reduction with the prediction of urban expansion, the predicted urban areas can effectively avoid areas that are highly vulnerable to floods and earthquakes. The total flood and earthquake losses in terms of area confirmed that losses in urban areas will be reduced by using the master plan with flood and earthquake risk instead of just using the master plan. By using different features with the prediction model, multiple scenarios of predicted urban areas can be available to support decision-making or policies that can reduce flood and earthquake risk.

References:
[1] I. Morley, "Rangoon," Cities. Vol.31, pp. 601-614, 2013. J. Clerk Maxwell, "A Treatise on Electricity and Magnetism," 3rd ed., Vol.2, Oxford: Clarendon, pp. 68-73, 1892.

[2] United Nations, "World Urbanization Prospects (The 2014 Revision)," Department of Economic and Social Affairs, Population Division, 2015.

[3] JICA (Japan International Cooperation Agency), "The Project for

the Strategic Urban Development Plan of the Greater Yangon," 2013.

[4] http://www.mmtimes.com/index.php/national-news/yangon/17012-Yangon-flood-losses-top-k11-billon.html [accessed June 20, 2016]

[5] World Bank, "Myanmar Southeast Asia Disaster Risk Management Project," 2017.

[6] I. S. Lowry, "A model of metropolis Santa Monica," CA (Rand Corporation), 1964.

[7] F. H. Sklar and R. Costanza, "The development of dynamic spatial models for landscape ecology," A review and prognosis, pp. 239-288, 1991.

[8] M. Batty, "Cellular automata and urban form," J. of the American Planning Association. Vol.63, No.3, pp. 264-274, 1997.

[9] I. Benenson, "Multiagent simulations of residential dynamics in the city," Computers Environment and Urban Systems. Vol.22, No.1, pp. 25-42, 1998.

[10] X. Zhang and Y. Wang, "Spatial dynamic modeling for urban development," Photogrammetric engineering and remote sensing. Vol.67, No.9, pp. 1049-1057, 2001.

[11] T. Sritarapipat and W. Takeuchi, "Building Classification in Yangon City, Myanmar using Stereo GeoEye Images, Landsat Image and Night-time Light Data," Remote Sensing Applications: Society and Environment, Vol.6, pp. 46-51, 2017.

[12] S. H. Cho, Z. Chen, S. T. Yen, and D. B. Eastwood, "Estimating effects of an urban growth boundary on Land development," J. of Agricultural and Applied Economics, Vol.38, No.2, pp. 287-298, 2006.

[13] T. Sritarapipat and W. Takeuchi, "Urban growth modeling based on the multi-centers of the urban areas and land cover change in Yangon, Myanmar," J. of Remote Sensing Society of Japan, Vol.37, No.3, pp. 248-260, 2017.

[14] D. Hoornweg and K. Pope, "Socioeconomic Pathways and Regional Distribution of the World's 101 Largest Cities," Global Cities Institute, Working Paper No.4, 2014.

[15] N. Kazakis, I. Kougias, and T. Patsialis, "Assessment of flood hazard areas at a regional scale using an index-based approach and Analytical Hierarchy Process: Application in Rhodope – Evros region, Greece," Science of the Total Environment, Vol.538, pp. 555-563, 2015.

[16] S. Karimzadeh, M. Miyajima, R. Hassanzadeh, R. Amiraslanzadeh, and B. Kamel, "A GIS based seismic hazard, building vulnerability and human loss assessment for the earthquake scenario in Tabriz," Soil Dynamics and Earthquake Engineering. Vol.66, pp. 263-280, 2014.

[17] M. Thant, "Probabilistic Seismic hazard assessment for Yangon region, Myanmar," ASEAN Engineering J. Part C, Vol.3, No.2, p. 131, 2012.

[18] W. Kron, "Flood Risk = Hazard·Values·Vulnerability," Water Int., Vol.30, pp. 58-68, 2005.

[19] JICA (Japan International Cooperation Agency), "The Strategic Urban Development Plan and the Urban Transport Development Plan of the Greater Yangon," 2016.

Name:
Tanakorn Sritarapipat

Affiliation:
Doctoral Student, Institute of Industrial Science, The University of Tokyo

Address:
6-1, Komaba 4-chome, Meguro, Tokyo 153-8505, Japan
Brief Career:
2009-2011 Programmer, The Center for Promoting Research and Development of Satellite Image Applications in Agriculture, Kasetsart University, Thailand
2011-2014 Researcher, Geo-Informatics and Space Technology Development Agency (GISTDA), Thailand
2014-Present Doctoral Student, Civil Engineering, The University of Tokyo, Japan
Selected Publications:
● Sritarapipat and W. Takeuchi, "Urban growth modeling based on the multi-centers of the urban areas and land cover change in Yangon, Myanmar," J. of Remote Sensing Society of Japan, Vol.37, No.3, pp. 248-260, 2017.
● T. Sritarapipat and W. Takeuchi, "Building Classification in Yangon City, Myanmar using Stereo GeoEye Images, Landsat Image and Night-time Light Data," Remote Sensing Applications: Society and Environment, Vol.6, pp. 46-51, 2017.
● T. Sritarapipat, P. Rakwatin, and T. Kasetkasem, "Automatic rice crop height measurement using a field server and digital image processing," Sensors, Vol.14, No.1, pp. 900-926, 2014.
● T. Sritarapipat, T. Kasetkasem, and P. Rakwatin, "Fusion and registration of THEOS multispectral and panchromatic images," Int. J. of Remote Sensing, Vol.35, No.13, pp. 5120-5147, 2014,

Name:
Wataru Takeuchi

Affiliation:
Associate Professor, Institute of Industrial Science, The University of Tokyo

Address:
6-1 Komaba 4-chome, Meguro, Tokyo 153-8505, Japan

Brief Career:
2004-2005 Post Doctoral Fellow, Institute of Industrial Science, University of Tokyo, Japan
2005-2006 Research Associate, Institute of Industrial Science, University of Tokyo, Japan
2007-2010 Assistant Professor, Institute of Industrial Science, University of Tokyo, Japan
2007-2007 Short Time Expert (Remote sensing and GIS) of Japanese International Cooperation Agency (JICA), Asian Institute of Technology, Thailand
2007-2009 Visiting Assistant Professor, Asian Institute of Technology, Thailand
2007-2009 Coordinator, Regional Network Office for Urban Safety (RNUS) of IIS, Asian Institute of Technology, Thailand
2010-2012 Director, Bangkok Office, Japan Society for Promotion of Science (JSPS)
2010-present Associate Professor, Institute of Industrial Science, University of Tokyo, Japan

Selected Publications:
● P. Misra, A. Fujikawa, and W. Takeuchi, "Novel decomposition scheme for characterizing urban aerosols observed from MODIS," Remote Sens, Vol.9, No.8, p. 812, 2017.
● A. Hirata, K. Nakamura, K. Nakao, Y. Kominami, N. Tanaka, H. Ohashi, K. T. Takano, W. Takeuchi, and T. Matsui, "Potential distributions of pine wilt disease under future climate change scenarios," PLoS ONE, Vol.12, No.8.
● T. Sritarapipat and W. Takeuchi, "Urban growth modeling based on the multi-centers of the urban areas and land cover change in Yangon, Myanmar," J. of Remote Sensing Society of Japan, Vol.37, No.3, pp. 248-260, 2017.
● M. Adachi, A. Ito, S. Yonemura, and W. Takeuchi, "Estimation of global soil respiration by accounting for land-use changes derived from remote sensing data," J. of Environmental Management, Vol.200, pp. 97-104, 2017.
● T. Sritarapipat and W. Takeuchi, "Building Classification in Yangon City, Myanmar using Stereo GeoEye Images, Landsat Image and Night-time Light Data," Remote Sensing Applications: Society and Environment, Vol.6, pp. 46-51, 2017.
● S. Kakuta, W. Takeuchi, and A. Prathep, "Seaweed and seagrass mapping in Thailand measured by using Landsat 8 optical and texture properties," J. of Marine Science and Technology, Vol.24, No.6, pp. 1155-1160, 2016.
● N. M. Yusoff, F. M. M., W. Takeuchi, S. Darmawan, and M. H. A. Razak, "Phenology and classification of abandoned agricultural land based on ALOS-1 and 2 PALSAR multi-temporal measurements," Int. J. of Digital Earth, 2016.
● L. Xi and W. Takeuchi, "Land surface water coverage estimation with PALSAR and AMSR-E for large scale flooding detection," Terrestrial, Atmospheric and Oceanic Sciences, Vol.27, No.4, pp. 473-480, 2016.
● P. Misra and W. Takeuchi, "Air quality analysis using nighttime light for Indian urban regions," Malaysian J. of Remote Sensing, Vol.5, No.2, pp. 119-126, 2016.
● S. Darmawan, W. Takeuchi, H. Abidin, M. N. Rasid, and M. N. Samat, "An investigation of age and yield of fresh fruit bunches of oil palm based on ALOS PALSAR2," Malaysian J. of Remote Sensing, Vol.5, No.2, pp. 57-65, 2016.

Academic Societies & Scientific Organizations:
● American Society for Photogrammetry and Remote Sensing (ASPRS)
● American Geophysical Union (AGU)
● Remote sensing society of Japan (RSSJ)
● Japan society of photogrammetry and remote sensing (JSPRS)